Spherical Symmetric Diffusion Problem

EVGENII B. KRISSINEL'

Institute of Water and Environmental Problems, Siberian Branch of the Russian Academy of Sciences, Papanintsev St. 105, Barnaul 656099, Russia

NOAM AGMON*

Department of Physical Chemistry and the Fritz Haber Research Center, The Hebrew University, Jerusalem 91904, Israel

Received 6 April 1995; accepted 10 October 1995

ABSTRACT

We introduce a general and versatile MS Windows application for solving the spherically symmetric diffusion problem, involving up to two coupled spherically symmetric Smoluchowski equations. The application is based on a modular, configurable, user-friendly graphical interface, in which input parameters are introduced through a graphical representation of the system of partial differential equations and output attributes can be obtained graphically during propagation.

The numerical algorithm consists of finite differencing in space and Chebyshev propagation in time; it includes an implementation of virtual gridding, which enhances the accuracy of calculating boundary conditions and steep potentials. The program has been checked against a wide collection of analytical solutions and applied to an experimentally open problem in excited-state proton-transfer to solvent.

Physical Background

The diffusion equation has been widely applied to heat conduction problems for over a century.[1] Its generalization to the case of an interaction potential by Smoluchowski[2] and its application by Debye[3] have paved the road to its widespread popularity in chemistry and biophysics. The approach is much simpler than full molecular dynamics, but, unlike phenomenological rate equations, takes into account the spatial geometry. The simplest geometry is that of spherical symmetry. The spherically symmetric diffusion problem (SSDP) has a wide variety of applications, depending on dimensionality, boundary conditions, initial distribution, diffusivity, interaction potentials, sink, and coupling terms.

The simplest case is diffusion on an infinite line without boundaries. The solution for a harmonic potential with an initial delta-function distribution was first obtained by Ornstein and Uhlenbeck.[4,5] It

*Author to whom all correspondence should be addressed.

CCC 0192-8651 / 96 / 091085-14

may describe a nonreactive relaxation process. The case of a double-well potential corresponds to the well known Kramers barrier-crossing problem.[6,7] The parabolic problem with an added delta-function sink at the potential minimum[8,9] has been used to describe barrierless isomerization in solution.[10,11]

More complicated potentials and sink terms have also been considered.[12] A spherically symmetric rate function may depict ligand binding to heme proteins.[13,14] The diffusion space (DS) then represents fluctuating protein conformations. In models for electron transfer in solution it represents solvent conformations.[15,16] When the reaction is reversible, two DSs are required to model environmental fluctuations in the reactants' and products' states, which are coupled by two coordinate-dependent rate functions.[17-19]

Chemical reactivity can also be described by boundary conditions. The dissociation of a diatomic molecule is modeled[20,21] as biased random walk along the vibrational ladder with an absorbing boundary at the dissociation level. This is approximately equivalent to diffusion in energy space with a linear "potential" and reflecting and absorbing boundaries at the two ends.[22]

Bimolecular reactions in solution correspond to a three-dimensional version of the SSDP.[23] The simplest reaction involves recombination at contact. Infinitely fast recombination is depicted by an absorbing boundary condition, whereas finite reaction rates are mimicked by the radiation boundary condition.[24] This provides a convenient means for modeling irreversible geminate recombination.[25-27] Noncontact reactivity, with distance-dependent sink terms, is important for electron transfer between geminate partners.[28] Likewise, distance-dependent Förster quenching describes energy transfer between two diffusing molecules or chromophores at the ends of a biopolymer.[29,30] For reversible geminate pairs, this may be generalized to the back-reaction boundary condition.[31,32] Reversible proton transfer to solvent has been analyzed using this boundary condition and a Coulomb potential.[33] Time-resolved fluorescence from excited hydroxypyrene-trisulfonate (HPTS) proved to be an ideal test case for this model.[34,35]

A geminate reaction need not occur on a single electronic potential surface. Two coupled Smoluchowski equations are needed for a complete description of the time evolution in two electronic states. For example, the excited HPTS molecule which dissociates reversibly in S_1, decays radiatively to the ground S_0 state, where it recombines irreversibly with the proton. The overall recombination rate coefficient[36] and the escape yield,[37,38] but not the complete time behavior, have been determined experimentally using ground-state absorption. Spin-dependent recombination also involves two coupled DSs: for the triplet and the singlet states.[39,40] The coupling now arises from intersystem crossing. Similarly, the description of geminate ion–electron pair recombination may require two DSs: for the "dry" and solvated electron. Solvation is depicted as a rate process which couples the two Smoluchowski equations.[41]

Nongeminate reactions are simplified in the pseudo-unimolecular case. One important class of irreversible pseudo-unimolecular reactions involves fluorescence quenching,[42,43] where the Smoluchowski theory is expected to provide a good approximation to the quenching kinetics. Here the many-body problem reduces to a calculation of the recombination flux $k(t)$ for a geminate pair. More complicated many-body effects occur in a two-step irreversible reaction, such as forward electron transfer in the excited state followed by backward transfer in the ground state.[44] This may be formulated as an effectively single-particle SSDP, for two coupled DSs.[45,46]

Many-body effects occur in pseudo-unimolecular reversible reactions. For example, proton transfer from HPTS shows an interesting pH dependence of its transient fluorescence signal, possibly due to proton–proton competition over binding.[47] The exact problem is isomorphic to multidimensional diffusion.[48] In practice, one employs mean-field approximations such as the superposition approximation.[49] This is again an effective pair-like SSDP, albeit with a nonlinear dissociation term.[50]

In the following text we introduce a single computational scheme capable of solving all of the above problems and more.

Goals

Our goal was to write a versatile program which may be configured to solve each of the above-mentioned problems. This program should be driven by a user-friendly graphical user interface (GUI) that has the following characteristics:

- **a.** Scientific accuracy: Tested in comparison with available analytic solutions.
- **b.** Modularity: A hierarchy of coupled differential equations may be unfolded when required.

c. Graphical input: The main screen, into which the parameters are entered, is a symbolic graphical representation of the system of coupled partial differential equations.
d. Versatility: Input is allowed as constants, user-defined functions, or data files.
e. Graphical output display.
f. Easy to use, menu-driven software.

The program we describe, SSDP version 1.4, is an MS Windows application written in Borland C++ 4.0 on the basis of Borland's Object Window Library (OWL) 1.0. We believe this program could serve as a useful tool in analyzing kinetic data in experimental laboratories worldwide.

Equations

DIFFUSIONAL HIERARCHY

SSDP solves up to three levels of coupled differential equations. Level 1 is always a diffusion space (DS) and level 2 may be either a DS or a discrete state. Level 3 is limited to a single discrete state. For DS1 and DS2 the space (r) and time (t) evolution of the density function at level i, $p_i(r, t)$, is given by the spherically symmetric Smoluchowski equation

$$\partial p_i(r,t)/\partial t = \mathscr{L}_i p_i(r,t) - \left[w_i(r) + \sum_{j\neq i} k_{ij}(r)\right] p_i(r,t) + \sum_{j\neq i} k_{ji}(r) p_j(r,t), \quad i = 1 \text{ or } 2 \qquad (1)$$

to be solved between two concentric spheres, $a \leq r \leq A$. The Smoluchowski operator in d dimensions is defined by

$$\mathscr{L}_i \equiv r^{1-d} \frac{\partial}{\partial r} r^{d-1} D_i(r) e^{-V_i(r)} \frac{\partial}{\partial r} e^{V_i(r)} \qquad (2)$$

The (spherically symmetric) interaction potential at level i is $U_i(r)$ and $V_i(r) \equiv U_i(r)/k_B T$, where k_B is Boltzmann's constant and T is the absolute temperature. $D_i(r)$ and $w_i(r) \equiv k_{ii}(r)$ are the diffusion coefficient and sink term at level i, respectively. Coupling between the levels is due to $k_{ij}(r)$, the reaction rate from level i to j at the given value of the radius vector r. Whenever just a single DS is considered, we omit the subscripts.

Level 3 is always a discrete state, while level 2 may be a discrete state instead of a DS. Whenever level j is discrete rather than a continuous DS, the notations change to reflect the unit change. Thus the term $k_{ji}(r)p_j(r, t)$ in eq. (1) changes to $K_{ji}(r)P_j(t)$, where P_j is the probability of discrete state j and K_{ji} denotes transitions to a continuous DS, i. Discrete states obey an ordinary differential equation

$$dP_i(t)/dt = \gamma_d \sum_{j\neq i} \int_a^A r^{d-1}\, dr \left[k_{ji}(r) p_j(r,t) - K_{ij}(r) P_i(t)\right] \qquad (3)$$

The geometric factor $\gamma_d \equiv 2\pi^{d/2}/\Gamma(d/2) = 2, 2\pi$, and 4π for $d = 1$, 2, and 3, respectively. For $d = 1$ it is divided by 2 (i.e., $\gamma_1 = 1$), assuming reaction from only one side of the boundary.

BOUNDARY CONDITIONS

For each DS, boundary conditions (BC) must be specified at $r = a$ and $r = A$. Either the probability density or the flux

$$J_i(r,t) \equiv -\gamma_d r^{d-1} D_i(r) e^{-V_i(r)} \frac{\partial}{\partial r} e^{V_i(r)} p_i(r,t) \qquad (4)$$

are prescribed at the boundary. Several boundary conditions might be considered. These are exemplified at $r = a$:

a. Absorbing boundary, $p_i(a, t) = 0$.
b. Constant concentration, $p_i(a, t) = c$.

(An absorbing boundary is a special case when $c = 0$.)

c. Reflecting boundary, $J_i(a, t) = 0$.
d. The "radiation" BC,[24]

$$J_i(a,t) = -\kappa_a^i p_i(a,t) \qquad (5)$$

where $\kappa_a \equiv \gamma_d a^{d-1} \kappa_r$. (Reflecting and absorbing boundaries are special cases when $\kappa_r = 0$ and ∞, respectively.)

e. The "back-reaction" BC,

$$J_i(a,t) = \kappa_d^i P_i(t) - \kappa_a^i p_i(a,t) \qquad (6)$$

where a dissociation term with a rate parameter κ_d has been added to the radiation boundary condition.[31,32] Note that each level i may have a different BC imposed at $r = a$ (and $r = A$) with different dissociation and

recombination rate parameters κ_d^i and κ_r^i. We omit the index i when only one DS is involved or in general relations that hold irrespective of i.

Fluxes emanating from boundaries and sinks are collected in each level in a "product state" P_i and an "escape state" E_i. This nomenclature originates in the field of geminate recombination, where P_i is the geminate recombination yield and E_i is the yield of pairs separated to very large distances. In the most general case presented so far—that of the back-reaction BC—these states obey the following differential equations:

$$\begin{aligned} dP_i(t)/dt &= \kappa_a^i p_i(a,t) - \kappa_d^i P_i(t) \\ &\quad + \gamma_d \int_a^A w_i(r) p_i(r,t) r^{d-1}\, dr \\ &\quad - \sum_{j\neq i} k_{ij}^a P_i(t) + \sum_{j\neq i} k_{ji}^a P_j(t) \\ dE_i(t)/dt &= \kappa_A^i p_i(A,t) - \kappa_e^i E_i(t) \\ &\quad - \sum_{j\neq i} k_{ij}^A E_i(t) + \sum_{j\neq i} k_{ji}^A E_j(t). \quad (7) \end{aligned}$$

Thus the product state collects the density exiting the DS through the $r = a$ boundary as well as from the coordinate-dependent sink term $w(r)$. The escape state collects only flux exiting the DS at $r = A$. Here κ_A and κ_e are the analogs of κ_a and κ_d at $r = A$. In addition, transitions between product states of different levels are incorporated via the rate constants k_{ij}^a. Similarly, transitions between escape states of different levels are incorporated via the rate constants k_{ij}^A.

A discrete i ($i = 2$ or 3) is treated as a DS which has degenerated into a single product state $P_i(t)$. Its time dependence is given by eq. (3), generalized to include also transitions to/from other product and escape states

$$\begin{aligned} &dP_i(t)/dt \\ &= \gamma_d \sum_{j\neq i} \left\{ \int_a^A r^{d-1}\, dr \left[k_{ji}(r) p_j(r,t) \right.\right. \\ &\quad \left. - K_{ij}(r) P_i(t) \right] \\ &\quad \left. + k_{ji}^a P_j(t) + k_{ji}^A E_j(t) - \left(k_{ij}^a + k_{ij}^A \right) P_i(t) \right\}. \quad (8) \end{aligned}$$

The inclusion of the product and escape states facilitates checking "mass-balance" conservation. For example, for normalized distributions we must have

$$\sum_i \left[P_i(t) + \gamma_d \int_a^A p_i(r,t) r^{d-1}\, dr + E_i(t) \right] = 1. \quad (9)$$

Thus, the DSs together with the product and escape states become a closed system. If level i is a discrete state, it contributes only the term $P_i(t)$ to this sum. For unnormalized distributions with a concentration BC the system is "open" namely, not all kinetic states are explicitly included. In this case, mass-balance conservation takes into account the density entering from the "bulk" through the appropriate boundary.

Finally, we allow for "generalized back-reaction" BC, in which κ_a and κ_d may be replaced by more complicated, time-dependent expressions. This dependence may be either explicit or implicit through other kinetic functions. For example, one may consider an effective pair approximation for the case of a uniform concentration c. Thus, the superposition approximation (SA) for treating many-body effects in reversible pseudo-unimolecular reactions[49] may be expressed as a SSDP with a single DS and the following BC:[50]

$$\begin{aligned} J(a,t) &= \kappa_d [\exp(cP(t)) - 1]/c - \kappa_a p(a,t) \\ p(A,t) &= 1 \quad (10) \end{aligned}$$

provided that A is taken sufficiently large. The initial (unnormalized) distribution is then $p(r,0) = \exp[-V(r)]$, where $V(r) \to 0$ as $r \to \infty$.

INITIAL DISTRIBUTION

Initial population may be on any level or divided between several levels. In each level, it may have continuous (DS) and discrete parts (product and escape states). The continuous part may be a delta function

$$p_i(r,0) = \delta(r - r_0)/(\gamma_d r_0^{d-1}) \quad (11)$$

the equilibrium distribution

$$p_i(r,0) = \exp(-V_i(r)) \quad (12)$$

or any other positive function of r. The initial distribution may be normalized, in which case eq. (9) is imposed at $t = 0$, or unnormalized as for the SA. An example of an unnormalized distribution is a uniform distribution $p(r,0) = 1$ over an unbound regime.

CALCULATED ATTRIBUTES

From the density profiles $p_i(r,t)$, obtained by solving the SSDP, the following kinetic attributes may be calculated:

a. The survival probability

$$S_i(t) \equiv \gamma_d \int_a^A p_i(r,t) r^{d-1}\, dr \qquad (13)$$

b. The recombination and escape probabilities $P_i(t)$ and $E_i(t)$ with their corresponding rates $dP_i(t)/dt$ and $dE_i(t)/dt$, respectively.

c. The "Kramers' survival"

$$S_i^K(t) \equiv \gamma_d \int_{r_1}^{r_2} p_i(r,t) r^{d-1}\, dr \qquad (14)$$

which is restricted to a subspace $[r_1, r_2]$ of the DS, namely, $a \le r_1 \le r_2 \le A$.

d. The average separation (first moment of r)

$$\langle r \rangle_i(t) \equiv \gamma_d \int_a^A p_i(r,t) r^d\, dr \qquad (15)$$

e. The average square separation (second moment of r)

$$\langle r^2 \rangle_i(t) \equiv \gamma_d \int_a^A p_i(r,t) r^{d+1}\, dr \qquad (16)$$

Numerical Algorithm

The numerical algorithm applied is that described in Section III of ref. 33 with minor improvements. It utilizes a spatial finite-differencing scheme that obeys detailed balancing[13] with a Chebyshev time propagation.[51] This propagation scheme is very accurate and allows for large time steps. The spatial finite-differencing operator is equivalent to a tridiagonal nearest-neighbor transition matrix. It obeys detailed balancing; therefore, the equilibrium distribution is precisely its lowest eigenstate, so that long-time propagations do not result in accumulating errors. It also preserves mass balance (i.e., state probabilities) to within the numerical accuracy (double precision, 14 digit).

The finite-differencing operator is faster to evaluate (on the order of N operations for N grid points), but much less accurate than spectral methods.[52] In comparison with analytic solutions (see Appendix), a maximal four-digit agreement is obtained at times corresponding to the center of the operator's eigenvalue spectrum using $N = 100$ grid points. The agreement deteriorates for steep potentials, requiring the use of denser spatial grids.

VIRTUAL GRIDDING

Our finite-differencing scheme incorporates a novel "virtual-gridding" (VG) strategy, resulting in a more accurate treatment of boundary conditions and rapidly varying potentials for a given number of grid points. In this method, transition probabilities between the N actual grid points are estimated using an additional set of $N + 1$ virtual points interleaving the actual grid. The procedure may be motivated by analogy with chemical kinetics: The finite differencing produces a set of rate equations for transitions between the actual states. The virtual states are like chemical intermediates under steady-state conditions.

Consider fixed-size gridding Δr for a DS $a \le r \le A$ using N actual grid points. Setting $\Delta r = (A - a)/N$, one places the grid points $1, 2, \ldots, N$ so that $r_1 = a + \Delta r/2$, $r_2 = a + 3\Delta r/2, \ldots$, and $r_N = A - \Delta r/2$. This grid is augmented with $N + 1$ VG points of half-integer indices, $1/2$, $3/2, \ldots, N + 1/2$ located at $r_{1/2} = a$, $r_{3/2} = a + \Delta r, \ldots$, and $r_{N+1/2} = A$. Thus the boundaries are VG points. Define the radial density function by $q(r,t) \equiv \gamma_d r^{d-1} p(r,t)$ and denote

$$q_j(t) = q(r_j, t)\Delta r \qquad (17)$$

a pure number.

The virtual-gridding assumption is that transitions from point i to an actual nearest-neighboring point $i + 1$ (or $i - 1$) occurs through the VG point $i + \frac{1}{2}$ (or $i - \frac{1}{2}$) under steady-state conditions

$$\begin{aligned} 0 &= dq_{i+1/2}(t)/dt \\ &= \omega(i \to i + \tfrac{1}{2}) q_i(t) + \omega(i + 1 \to i + \tfrac{1}{2}) q_{i+1}(t) \\ &\quad - [\omega(i + \tfrac{1}{2} \to i - 1) + \omega(i + \tfrac{1}{2} \to i + 1)] \\ &\quad \times q_{i+1/2}(t) \end{aligned} \qquad (18)$$

This gives an expression for $q_{i+1/2}(t)$ in terms of $q_i(t)$ and $q_{i+1}(t)$. The $i \to i \pm \frac{1}{2}$ transition frequencies are given by[13]

$$\omega(i \to j) = D(r_j - r_i)^{-2} (r_j/r_i)^{(d-1)/2} \times \exp\left(\left[V(r_i) - V(r_j)\right]/2\right) \qquad (19)$$

For half-integer transitions $(r_j - r_i)^2 = \Delta r^2/4$.

Starting from the master equation for dq_i/dt in terms of its two nearest virtual neighbors and using eq. (18) at $i \pm \frac{1}{2}$, we find for any interior point $(1 < i < N)$ that

$$dq_i(t)/dt = \omega(i - \tfrac{1}{2} \to i)q_{i-1/2}(t) + \omega(i + \tfrac{1}{2} \to i)q_{i+1/2}(t) - [\omega(i \to i - \tfrac{1}{2}) + \omega(i \to i + \tfrac{1}{2})]q_i(t) \quad (20a)$$

$$= \Omega(i - 1 \to i)q_{i-1}(t) + \Omega(i + 1 \to i)q_{i+1}(t) - [\Omega(i \to i - 1) + \Omega(i \to i + 1)]q_i(t) \quad (20b)$$

where the $i \to i \pm 1$ transition frequencies are given by

$$2\Omega(i \to i \pm 1) = \frac{\omega(i \to i \pm \frac{1}{2})\omega(i \pm \frac{1}{2} \to i \pm 1)}{\omega(i \pm \frac{1}{2} \to i) + \omega(i \pm \frac{1}{2} \to i \pm 1)} \quad (21)$$

In chemical kinetics this represents a well known formula for the rate constant of two consecutive reaction steps. For $V = 0$ and $d = 1$ all transition probabilities are the same as obtained in the regular (non-VG) scheme and equal $D/\Delta r^2$. For a nonvanishing potential the VG method samples $V(r)$ at both integer and half-integer grid points; hence, its improved accuracy.

The situation at the boundaries depends on the BC imposed there. Let us consider the back-reaction BC [eq. (6)] imposed at $r = a$. Absorbing, reflecting, or radiation BCs are special cases. BCs at $r = A$ are treated analogously. Let us assign an index 0 to the product state $q_0(t) \equiv P(t)$ and evaluate the transitions $1 \to 0$ and $0 \to 1$. Since the boundary is at $r_{1/2} = a$, we set[33]

$$\omega(0 \to \tfrac{1}{2}) = 2\kappa_d, \quad \omega(\tfrac{1}{2} \to 0) = 2\kappa_r/\Delta r. \quad (22)$$

The factor of 2 accounts for the half-grid spacing. Inserting into the general relation [eq. (21)] gives

$$\Omega(0 \to 1) = \kappa_d\omega(\tfrac{1}{2} \to 1)/[2\kappa_r/\Delta r + \omega(\tfrac{1}{2} \to 1)]$$
$$\Omega(1 \to 0) = \kappa_r\omega(1 \to \tfrac{1}{2})/[2\kappa_r + \omega(\tfrac{1}{2} \to 1)\Delta r] \quad (23)$$

with $\omega(\frac{1}{2} \to 1)$ calculated from eq. (19). This allows κ_r to be very large in comparison with the diffusion term. In particular, the absorbing boundary limit $\kappa_r \to \infty$ is calculated as $\Omega(1 \to 0) = \omega(1 \to \frac{1}{2})/2$. Unlike the ordinary gridding method, which leads to an infinite transition probability from the boundary, VG provides a finite transition probability from a point $\Delta r/2$ away from it. Thus eq. (23) provides a numerically correct presentation for boundary conditions.

VG TESTING

For (radiation, back-reaction) BCs our experience indicates that the VG relation [eq. (23)] gives good results. Therefore, it is the only procedure used to evaluate boundary transition frequencies.

The situation is more complicated regarding VG for the interior of the DS [eq. (21)]. Without an interaction potential, it is the same as the ordinary gridding method[33] for $d = 1$ and gives numerically similar results for $d > 1$. Differences arise for cases of sharply varying potentials. For a linear potential (Example 2 in the Appendix) it improves the behavior of the second moment, but not that of the first moment.

A calculation for a harmonic potential (Example 3 in the Appendix) is shown in Figure 1. The exact profiles [eq. (31)] are the bold curves. The parameter α was assigned a sufficiently large value that 100 grid points are insufficient to produce an accurate result. While both regular (dashed curves) and VG methods (dotted curves) produce inaccurate results, VG seems to give better density profiles.

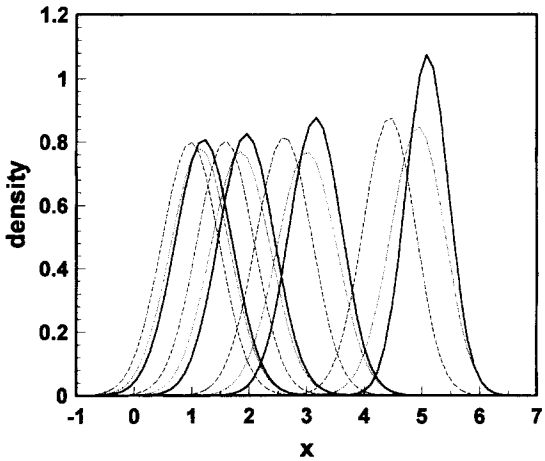

FIGURE 1. Profiles for the Ornstein–Uhlenbeck problem at four different times starting from a delta function at $r_0 = 8$; $N = 100$ and $\alpha = 4$. Bold curves denote analytic solution eq. (31); dashed and dotted curves denote ordinary and virtual gridding, respectively. The profiles may be smoothed using the `Spline` option.

The improvement is mainly in the first moment, namely, the location of the peaks. The second moment (the width) becomes less accurate than with ordinary gridding. Due to these mixed results, interior VG is implemented only as an option.

OPERATOR RANGE

An efficient Chebyshev propagation requires normalizing the interval of definition of the Chebyshev polynomials by the maximal eigenvalue of the operator.[51] If a finite-differencing operator is represented on a grid by a matrix (M_{ij}), its highest eigenvalue may be estimated from Gershgorin's theorem[53]

$$|\lambda_{max}| \leq \max_j \sum_i |M_{ij}| \quad (24)$$

For the special form of the tridiagonal finite-differencing operator,

$$|\lambda_{max}| \leq \max_j [\Omega(j \to j-1) + \Omega(j \to j+1) + \Omega(j-1 \to j) + \Omega(j+1 \to j)] \quad (25)$$

Graphical Interface

A versatile, general purpose program requires the input of a large number of parameters. The SSDP as described in Equations may involve up to three levels of coupled partial and ordinary differential equations. In each level one may specify the initial distribution, interaction potential, diffusion coefficient, sink term, boundary conditions, and coupling terms to other levels. Most of these attributes are functions of r, each depending on several parameters. Inputting that many parameters in a tabular format could be tedious and uninstructive. Our approach was to develop a dynamic graphical representation (DGR) of the coupled system of partial differential equations which is displayed in the main screen. The DGR changes its appearance as a function of the configuration of the specific problem to be solved. A quick glance at the main screen tells the user what kind of problem is considered.

The DGR of SSDP was built around the following concepts:

a. Only the activated levels are visible. When all transition probabilities to a DS of a lower level vanish, that level is not displayed.

b. The intra- and interlevel coupling (sink, rate) terms are depicted by two-state arrows. When activated (nonzero coupling) the arrows appear in bright colors; when null they appear in light hues. Clicking with the mouse opens a dialogue box that allows setting values (or functions) for the appropriate transition probability.

c. At each level, a geometric representation of the diffusion space (DS) is shown. For the present, spherically symmetric problem this is simply a radius vector. The boundaries of the DS can be clicked to change their location as well as the boundary condition imposed. The interior of the DS can be clicked to change the grid mesh. The discrete (product and escape) states also appear in two colors: dark and light for nonzero and zero initial population, respectively.

d. Auxiliary coordinate-dependent functions, such as potentials and initial distributions, are portrayed schematically as functions of the radius vector within (or above) the DS. The functions may be clicked to change parameters or functional dependencies, choosing from predefined or "user defined" functions via a built-in FORTRAN interpreter. These functions may be plotted more accurately in a special display screen.

e. The settings may be saved in a configuration file, allowing easy project retrieval. A library of configuration files for different problems has been prepared.

We demonstrate the DGR using a real research problem below.

Problem in Geminate Recombination

Hydroxypyrene-trisulfonate (HPTS) is a weak ROH acid in its ground electronic state, but a strong acid in the excited state, where it exhibits reversible, diffusion-influenced proton transfer to solvent (PTTS). While the excited-state fluorescence has been followed using time-correlated single-photon counting,[33-35] the ground-state recombination has not been monitored in the time domain. Only overall recombination rates[36] and the asymptotic yields[37,38] have been determined experimentally. We use SSDP to calculate both excited- and ground-state kinetics with the hope that the ground-state results will eventually be

tested by time-resolved nanosecond absorption measurements.

The overall reaction cycle involves excitation of the acidic form ROH to the vibrationally relaxed singlet state R*OH, which dissociates reversibly[33] to form R^*O^- and ultimately decays radiatively to the ground state where recombination is irreversible:

$$\begin{array}{ccc} R^*OH & \rightleftharpoons & R^*O^- + H^+ \\ \Uparrow \downarrow \tau_f & & \downarrow \tau_f' \\ ROH & \leftarrow & RO^- + H^+ \end{array} \qquad (26)$$

When analyzing fluorescence data, only the population in the excited state is relevant. If the fluorescence lifetimes are equal, $\tau_f = \tau_f'$, they may be ignored in the calculation. Subsequent comparison with experiment requires multiplying the calculated probabilities by $\exp(-t/\tau_f)$. The problem is describable on a single level.

The single-level DGR for the excited-HPTS kinetic is shown in Figure 2. The DS extends from the contact distance $a = 7$ Å to some sufficiently large value $A = 600$ Å to which no pairs separate on the time scale considered. This may be checked by setting the BC at $r = A$ to absorption and following the escape probability. $E(t)$ should be negligible, else A has to be increased. The initial state is the bound R*OH state. Hence the initial distribution in the DS vanishes while $P(0) = 1$. This is indicated by the dark color of the product state to the left of $r = a$. The BC at $r = a$ is reversible. The values of κ_r and κ_d appear on the appropriate button. The sink term $w(r)$ and the transitions to the ground state $k_{12}(r)$, k_{12}^a, and k_{12}^A all vanish, so that the four corresponding arrows are dimmed and the DS for ground-state pairs is not displayed. The interaction potential of the proton–R^*O^- pair is a Coulomb potential $V(r) = -R_D/r$, displayed schematically above the DS. It may be modified using the `Potential` button. Additional buttons allow setting the relative diffusion coefficient D, the number of grid points N, and the dimensionality, which is 3. The `Normalization: ON` setting imposes eq. (9) at $t = 0$.

The problem configured in Figure 2 has been solved numerically many times in the past[33-35] with parameters capable of fitting experiment from 10 ps to 10 ns. Using these parameters, one may predict the yet-to-be-measured kinetics on the ground electronic state. For that end, we solve the coupled excited-ground-state kinetics. The two-level hierarchy leads to the configuration shown in Figure 3. k_{12}^a is the radiative decay rate coefficient of R*OH while $k_{12}(r)$ is that of R^*O^-. Activating the two interlevel arrows opens DS2, in which we set $V_2(r) = V_1(r)$, $D_2 = D_1$, zero initial popula-

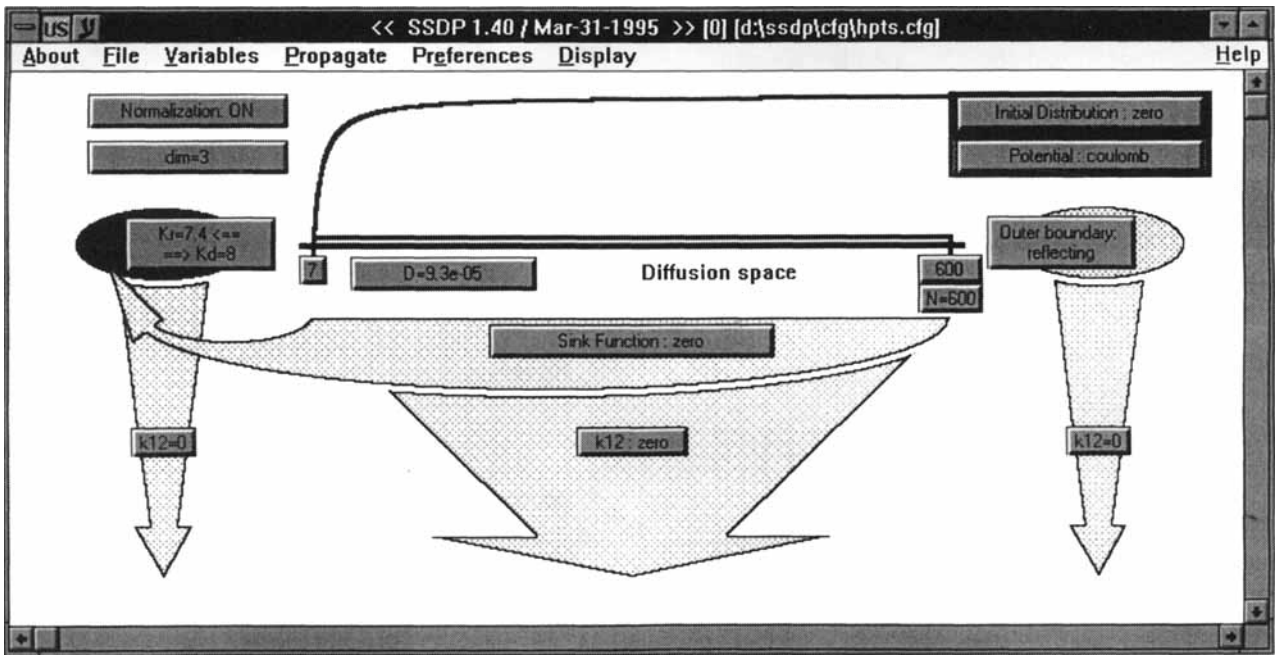

FIGURE 2. The main screen for the single-level HPTS problem.

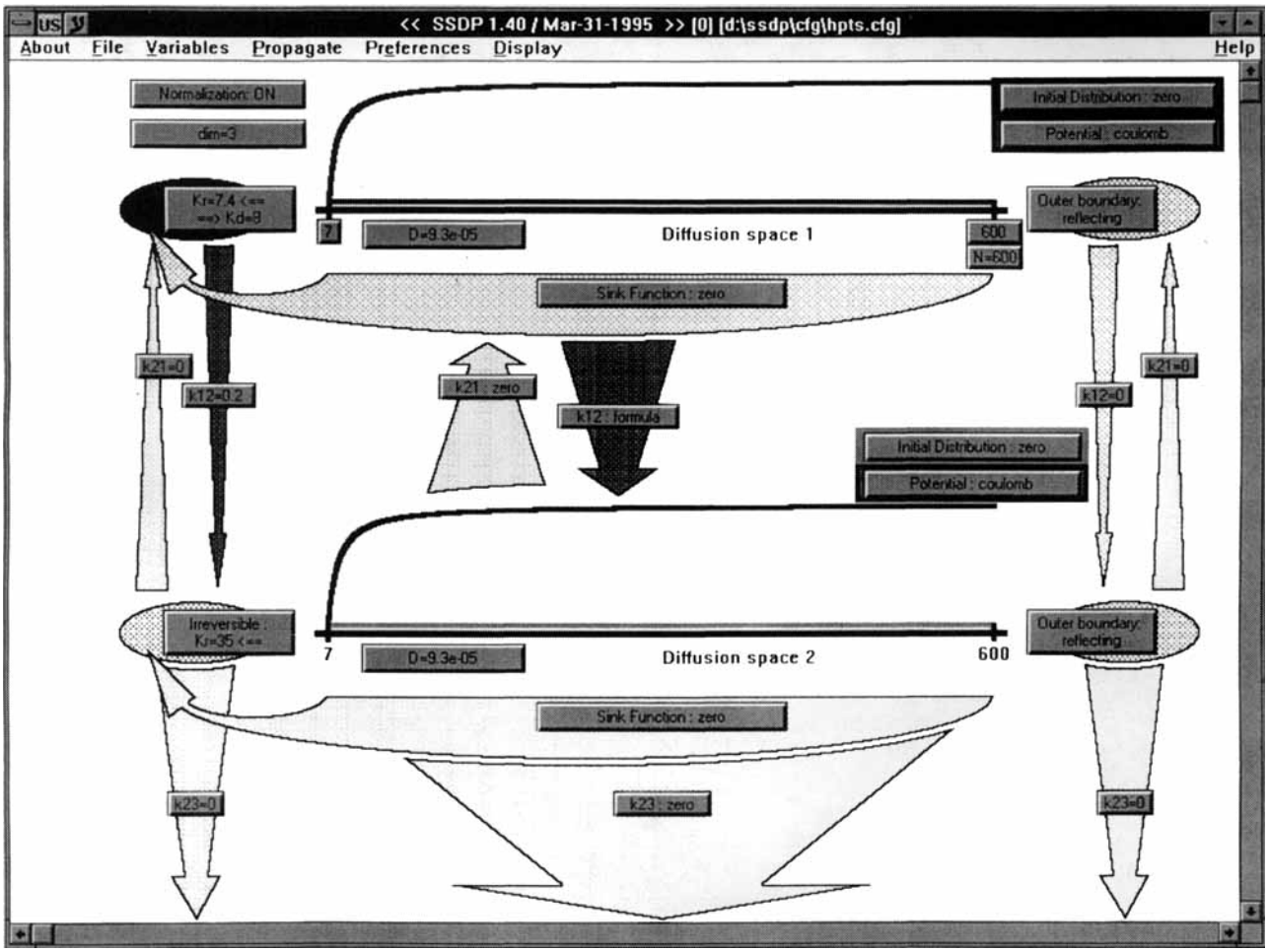

FIGURE 3. The main screen for the bilevel HPTS problem.

tion, and a radiation (irreversible) BC at $r = a$. κ_r^2 is estimated from the overall recombination rate coefficient k_{on} determined by Förster and Völker.[36]

Using these parameters, summarized in Table I, we calculate both excited (bold curves) and ground-state (dashed curves) kinetics, as shown in Figure 4. In the excited state, the initially excited R*OH decays rapidly while the R^*O^- signal builds up. When viewed on a log-log scale (not shown), the R*OH decay shows the expected $t^{-3/2}$ behavior. The present calculation focuses on longer times, when the R^*O^- radiative decay is coupled to the buildup of the ground-state population in the acidic (lower dashed curve) and basic (upper dashed curve) forms. The ultimate escape yield, the $t \to \infty$ limit of the RO^- signal, is about 0.76, in good agreement with the value of 0.74 ± 0.03 measured by Hauser et al. in pure water.[37] The com-

TABLE I.
Parameters for the Bilevel HPTS Problem.

$R_D^1 = R_D^2$ (Å)	$D_1 = D_2$ (Å² / ns)	κ_r^1 (Å / ns)	κ_d^1 (ns^{-1})	$1 / k_{12}^a$ (ns)	$1 / k_{12}(r)$ (ns)	κ_r^2 (Å / ns)	κ_d^2 (ns^{-1})
28.3	930	7.4	8	5	5.5	35	0

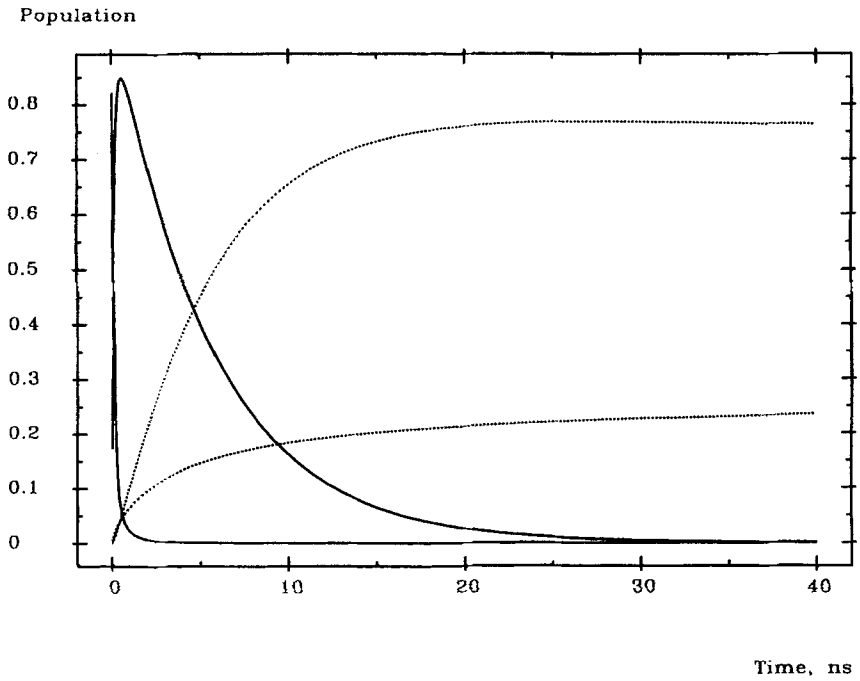

FIGURE 4. Kinetics of excited (bold curves) and ground-state (dashed curves) PTTS, calculated for the bilevel HPTS problem configured in Figure 3. On both levels, there is a larger probability to observe the anionic state at long times. Input parameters are given in Table I.

plete ground-state time behavior depicted in Figure 4 is a prediction that should be tested by transient absorption spectroscopy.

Conclusion

The SSDP 1.4 program introduced in this paper allows for the solution of a number of problems arising in experimental and theoretical research in the field of chemical kinetics, chemical physics, and elsewhere when one considers an interaction of particles on the background of their diffusional motion. The versatile interface developed allows the user to configure a problem and obtain meaningful results within just a few minutes. This may be especially important when several mathematical models need to be tested against experimental results.

We believe that SSDP 1.4 may be a useful tool in experimental and theoretical studies of diffusional kinetics. The simplicity of the interface and the built-in FORTRAN interpreter and help system makes it possible to use the program for educational purposes also. The program is available from the authors upon request together with a library of configuration files used to produce the results described in this paper.

In addition to the specific programming goals, SSDP is an exercise in developing user-friendly interfaces for systems of partial differential equations in chemistry. Problems of interest are not limited to diffusive dynamics. For example, an interface for coupled time-dependent Schrödinger equations for several electronic states may be developed along the lines of SSDP. To justify the extra effort that goes into a graphical package, the interface should be configurable to a wide family of related problems rather than solve a single equation. We have chosen to characterize such a "family" by a common underlying geometry (e.g., spherical symmetry). This allows to access the interior and boundaries of the spatial domain interactively and modify their attributes. A "hierarchy" of equations involving the same spatial domain may then be constructed. This hierarchy unfolds for nonvanishing coupling terms. We envisage the application of these concepts to problems extending beyond the immediate goals of SSDP.

Acknowledgments

Work supported by the US–Israel Binational Science Foundation (BSF), Jerusalem, Israel. The Fritz Haber Research Center is supported by the Minerva Gesellschaft für die Forschung, München, Germany.

Appendix: Analytic Solutions

In this appendix we provide a collection of analytic results that can be used to compare with numerical SSDP solutions. Such a comparison is vital. A comparison with a single case, like free diffusion, is insufficient because, depending on BCs, potentials, sink terms, and initial distributions, an algorithm may perform well in one limit but poorly in other limits. For example, the following situations might be problematic: boundary or sink reactivities much larger than diffusional rates, steeply varying potentials, delta-function initial distributions, nonlinear boundary conditions.

Examples are ordered by the complexity of the sink terms involved. BCs are equivalent to delta-function sinks.[54] Therefore, we first summarize results for problems involving no sinks whatsoever, then those involving only boundary sinks, and, finally, also distance-dependent sink terms. SSDP is capable of evaluating the analytic solutions as "user-defined functions" from within the program, thanks to a built-in FORTRAN interpreter.

NONREACTIVE DIFFUSION

The first set of examples involves a single infinite DS, $0 \le r < \infty$ ($-\infty < r$ for $d = 1$) with no population depletion. There are no boundary conditions (other than reflective) and no sink terms. The initial distribution is a delta function at r_0 [eq. (11)].

Example 1

Free diffusion, $V = 0$, in d dimensions; $r_0 = 0$. The profiles are given by

$$p(r,t) = (4\pi\, Dt)^{-d/2} \exp(-r^2/4\, Dt) \quad (27)$$

The moments are given by

$$\langle r \rangle = (4\, Dt)^{1/2}\Gamma((d+1)/2)/\Gamma(d/2)$$
$$\langle r^2 \rangle = 2d\, Dt \quad (28)$$

where Γ denotes the gamma function.[55] Here $\langle r \rangle$ is by integrating over $r \ge 0$ also when $d = 1$.

Example 2

Linear potential (diffusion with drift), $V(r) = \alpha r$, in $d = 1$. The profiles are given by

$$p(r,t) = (4\pi\, Dt)^{-1/2} \times \exp\left[-(r - r_0 + \alpha\, Dt)^2/4\, Dt\right] \quad (29)$$

The moments are given by

$$\langle r \rangle = r_0 - \alpha\, Dt$$
$$\langle r^2 \rangle = r_0^2 + 2\, Dt(1 - \alpha r_0) + (\alpha\, Dt)^2 \quad (30)$$

Example 3

The Ornstein–Uhlenbeck process. Diffusion in a harmonic potential, $V = \alpha r^2$, $d = 1$. The profiles are given by[4,5]

$$p(r,t) = [2\pi\sigma(t)^2]^{-1/2} \exp\left[-(r - \langle r \rangle)^2/2\sigma(t)^2\right] \quad (31)$$

The moments are given by

$$\langle r \rangle = r_0 \exp(-2\alpha\, Dt)$$
$$\langle r^2 \rangle = \frac{1}{2\alpha} + \left(r_0^2 - \frac{1}{2\alpha}\right)\exp(-4\alpha\, Dt)$$
$$\sigma(t)^2 \equiv \langle r^2 \rangle - \langle r \rangle^2 = [1 - \exp(-4\alpha\, Dt)]/2\alpha \quad (32)$$

Example 4

A reflective boundary condition (infinite potential wall) at $r = 0$ in $d = 1$. The density profile, obtainable by the method of images,[1] is

$$p(r,t) = (4\pi\, Dt)^{-1/2}\left[\exp\left(-(\zeta_1 - \zeta_0)^2\right) + \exp\left(-(\zeta_1 + \zeta_0)^2\right)\right] \quad (33)$$

Throughout the sequel we define

$$\zeta_0 \equiv (r_0 - a)/\sqrt{4\, Dt}$$
$$\zeta_1 \equiv (r - a)/\sqrt{4\, Dt} \quad (34)$$

ABSORBING BOUNDARY

A single semi-infinite DS, $a \le r < \infty$, with $p(a, t) = 0$, $w(r) = 0$, and an initial delta function at $r = r_0$. The following results may be obtained by the method of images.[1]

Example 5

$V = 0$ and $d = 1$. The density profile is[1]

$$p(r,t) = (4\pi Dt)^{-1/2}\left[\exp\left(-(\zeta_1 - \zeta_0)^2\right) - \exp\left(-(\zeta_1 + \zeta_0)^2\right)\right] \quad (35)$$

The survival probability is given by

$$S(t) = \mathrm{erf}(\zeta_0) \quad (36)$$

where erf is the error function.[55]

Example 6

$V = 0$ and $d = 3$. The survival probability is given by[1]

$$S(t) = 1 - \frac{a}{r_0}\mathrm{erfc}(\zeta_0) \quad (37)$$

where erfc is the complementary error function.[55]

Example 7

The "pinhole sink" at the bottom of a parabolic potential, $V = \alpha r^2$, in $d = 1$. The survival probability is given by[11]

$$S(t) = \mathrm{erf}\left(\sqrt{\alpha r_0^2/[\exp(4\alpha Dt) - 1]}\right) \quad (38)$$

Example 8

The same, for an initial equilibrium distribution. The survival probability is[8]

$$S(t) = 2\arcsin(\exp(-2\alpha Dt))/\pi \quad (39)$$

This result has been rederived several times in the literature.[9,16,11]

RADIATION BOUNDARY CONDITION

Same as above, with a "radiation" BC [eq. (5)] imposed at $r = a$.

Example 9

$d = 1$, initial delta function at $r = r_0$. The survival probability is[1,23]

$$S(t) = \mathrm{erf}(\zeta_0) + \exp(-\zeta_0^2)\mathrm{er}\left(\kappa_r\sqrt{t/D} + \zeta_0\right) \quad (40)$$

Here we have defined

$$\mathrm{er}(z) \equiv \exp(z^2)\mathrm{erfc}(z) \quad (41)$$

Example 10

Same as above, for a uniform initial distribution. The reaction rate (flux at $r = a$) is[56]

$$k(t) = \kappa_r\,\mathrm{er}\left(\kappa_r\sqrt{t/D}\right) \quad (42)$$

The density profiles in this case tend to a steady-state limit, $p(r, \infty)$, given by eq. (40) with r_0 replaced by r.

Example 11

Same as Example 9, in three dimensions. The density profile is given by

$$4\pi r_0^2 p(r,t) = \frac{r_0}{r\sqrt{4\pi Dt}}\left\{\exp\left(-(\zeta_1 - \zeta_0)^2\right) + \exp\left(-(\zeta_1 + \zeta_0)^2\right) \times\left[1 - \sqrt{4\pi}\,\xi\,\mathrm{er}(\zeta_0 + \zeta_1 + \xi)\right]\right\} \quad (43)$$

Here we have defined

$$a_{\mathrm{eff}} \equiv a\kappa_a/(4\pi Da + \kappa_a) = a^2\kappa_r/(D + a\kappa_r)$$
$$\xi \equiv \sqrt{Dt}/(a - a_{\mathrm{eff}}) \quad (44)$$

The survival probability is[1,24,23]

$$S(t) = 1 - \frac{a_{\mathrm{eff}}}{r_0}\left[\mathrm{erfc}(\zeta_0) - \exp(-\zeta_0^2)\mathrm{er}(\zeta_0 + \xi)\right] \quad (45)$$

Example 12

Same as above, for a uniform initial distribution. The reaction rate is[56,23]

$$k(t) = 4\pi Da_{\mathrm{eff}}[1 + \kappa_a\,\mathrm{er}(\xi)/(4\pi Da)] \quad (46)$$

The density profiles in this case tend to a steady-state limit, $p(r, \infty)$, given by eq. (45) with r_0 replaced by r.

BACK-REACTION BOUNDARY CONDITION

A single DS, $a \le r < \infty$, $d = 1$, $V = 0$, $w = 0$; a back-reaction BC [eq. (6)] at $r = a$. The solution is obtained for two different initial conditions[50]:

Example 13

Initially bound state: $P(0) = 1$ and $p(r,0) = 0$. The solution is

$$p(r,t) = \frac{\kappa_d}{\Delta} e^{-\zeta_1^2}\left[\mathrm{er}\left(\zeta_1 + \lambda_- \sqrt{t/D}\right) - \mathrm{er}\left(\zeta_1 + \lambda_+ \sqrt{t/D}\right)\right] \quad (47a)$$

$$P(t) = \left[\lambda_+ \mathrm{er}\left(\lambda_- \sqrt{t/D}\right) - \lambda_- \mathrm{er}\left(\lambda_+ \sqrt{t/D}\right)\right]/\Delta \quad (47b)$$

Here $\lambda_\pm \equiv (\kappa_r \pm \Delta)/2$ and $\Delta \equiv (\kappa_r^2 - 4D\kappa_d)^{1/2}$.

Example 14

Initially unbound state: $P(0) = 0$ and $p(r,0) = \delta(r - r_0)$. One obtains[32]

$$p(r,t) = (4\pi Dt)^{-1/2}\left\{\exp\left[-(\zeta_1 - \zeta_0)^2\right] + \exp\left[-(\zeta_1 + \zeta_0)^2\right]\right\} + \frac{\kappa_r}{D\Delta} e^{-(\zeta_0 + \zeta_1)^2}\left[\lambda_- \mathrm{er}\left(\zeta_0 + \zeta_1 + \lambda_- \sqrt{\frac{t}{D}}\right) - \lambda_+ \mathrm{er}\left(\zeta_0 + \zeta_1 + \lambda_+ \sqrt{\frac{t}{D}}\right)\right] \quad (48a)$$

$$P(t) = \frac{\kappa_r}{\Delta} e^{-\zeta_0^2}\left[\mathrm{er}\left(\zeta_0 + \lambda_- \sqrt{\frac{t}{D}}\right) - \mathrm{er}\left(\zeta_0 + \lambda_+ \sqrt{\frac{t}{D}}\right)\right] \quad (48b)$$

COORDINATE-DEPENDENT SINK TERMS

Here we cite some analytic solutions for coordinate-dependent sink terms.

Example 15

Free diffusion in one dimension, $V = 0$, $d = 1$, with $w(r) = (k/r)^2$ and an initial delta function at r_0. The density profile is given by[57]

$$p(r,t) = \frac{\sqrt{rr_0}}{2Dt} \exp\left(-\frac{r^2 + r_0^2}{4Dt}\right) I_\nu\left(\frac{rr_0}{2Dt}\right) \quad (49)$$

where I_ν is a modified Bessel function[55] of order ν where

$$\nu = \sqrt{k^2/D + 1/4} \quad (50)$$

Example 16

Parabolic potential, $V(r) = \alpha r^2$, and a parabolic sink term, $w(r) = \beta r^2$, in $d = 1$ for an initial equilibrium distribution. The survival probability is given by[58]

$$S(t) = \frac{\sqrt{8\gamma}\exp(-D\alpha(2-\gamma)t/\gamma)}{\sqrt{(2+\gamma)^2 - (2-\gamma)^2\exp(-4D\alpha t/\gamma)}} \quad (51)$$

where we have defined

$$\gamma \equiv 2/\sqrt{1 + \beta/D\alpha^2} \quad (52)$$

Example 17

The "lnch" potential $V(r) = -\ln(\cosh(r\sqrt{2\alpha}))$ with a parabolic sink term $w(r) = \beta r^2$ in $d = 1$. Initial delta function at r_0. The (conditional) moments are given by[59]

$$\frac{\langle r \rangle}{S(t)} = \frac{r_0}{\cosh(\tau)} + \sqrt{\frac{\alpha}{\beta}} \tanh(\tau) \tanh\left(\frac{\chi}{\cosh(\tau)}\right) \quad (53)$$

$$\frac{\langle r^2 \rangle}{S(t)} - \left[\frac{\langle r \rangle}{S(t)}\right]^2 = \frac{\alpha}{\beta}\left[\frac{\tanh(\tau)}{\cosh(\chi/\cosh(\tau))}\right]^2 + \frac{\tanh(\tau)}{\sqrt{2\beta}} \quad (54)$$

where $\tau \equiv t\sqrt{2\beta}$ and $\chi \equiv r_0\sqrt{2\alpha}$.

Example 18

Förster quenching $w(r) = \beta/r^6$ in three dimensions with no potential and a concentration bound-

ary condition $p(\infty, t) = 1$. The steady-state solution is[60]

$$p(r,\infty) = \frac{(2z)^{1/4}\pi}{\Gamma(1/4)I_{-3/4}(z_0)} \times \left[I_{-3/4}(z_0)I_{-1/4}(z) - I_{3/4}(z_0)I_{1/4}(z)\right] \quad (55)$$

where $z \equiv (\beta/D)^{1/2}/(2r^2)$ and $z_0 \equiv (\beta/D)^{1/2}/(2a^2)$.

References

1. H. S. Carslaw and J. C. Jaeger, *Conduction of Heat in Solids*, 2nd ed., Oxford University Press, Oxford, 1959.
2. M. V. Smoluchowski, *Ann. Phys.* **48,** 1103 (1915).
3. P. Debye, *Trans. Electrochem. Soc.*, **82,** 265 (1942).
4. G. E. Uhlenbeck and L. S. Ornstein, *Phys. Rev.* **36,** 823 (1930).
5. N. G. van Kampen, *Stochastic Processes in Physics and Chemistry*, North-Holland, Amsterdam, 1981.
6. H. A. Kramers, *Physica*, **7,** 284 (1940).
7. S. Chandrasekhar, *Rev. Mod. Phys.*, **15,** 1 (1943).
8. A. Szabo, K. Schulten, and Z. Schulten, *J. Chem. Phys.*, **72,** 4350 (1980).
9. A. Szabo, G. Lamm, and G. H. Weiss, *J. Statist. Phys.*, **34,** 225 (1984).
10. B. Bagchi, G. R. Fleming, and D. W. Oxtoby, *J. Chem. Phys.*, **78,** 7375 (1983).
11. B. Bagchi and G. R. Fleming, *J. Phys. Chem.*, **94,** 9 (1990).
12. U. Åberg et al., *Chem. Phys.*, **183,** 269 (1994).
13. N. Agmon and J. J. Hopfield, *J. Chem. Phys.*, **78,** 6947 (1983); erratum, **80,** 592 (1984).
14. N. Agmon and J. J. Hopfield, *J. Chem. Phys.*, **79,** 2042 (1983).
15. L. D. Zusman, *Chem. Phys.*, **49,** 295 (1980).
16. H. Sumi and R. A. Marcus, *J. Chem. Phys.*, **84,** 4894 (1986).
17. A. M. Berezhkovskii and V. Y. Zitserman, *Chem. Phys.*, **157,** 141 (1991).
18. J. Zhu and J. Rasaiah, *J. Chem. Phys.*, **95,** 3325 (1991).
19. J. Rasaiah and J. Zhu, *J. Chem. Phys.*, **98,** 1213 (1993).
20. E. W. Montroll and K. E. Shuler, *Adv. Chem. Phys.*, **1,** 361 (1958).
21. K. E. Shuler and G. H. Weiss, *J. Chem. Phys.*, **38,** 505 (1963).
22. N. Agmon, *J. Chem. Phys.*, **80,** 5049 (1984).
23. S. A. Rice, In *Computational Chemical Kinetics: Diffusion-Limited Reactions*, C. H. Bamford, C. F. H. Tipper, and R. G. Compton, Eds., Elsevier, Amsterdam, 1985, vol. 25.
24. F. C. Collins and G. E. Kimball, *J. Colloid Sci.*, **4,** 425 (1949).
25. A. G. Kofman and A. I. Burshtein, *Chem. Phys.*, **27,** 217 (1978).
26. H. Sano and M. Tachiya, *J. Chem. Phys.*, **71,** 1276 (1979).
27. M. Tachiya, *Radiat. Phys. Chem.*, **21,** 167 (1983).
28. A. I. Burshtein, A. A. Zharikov, and N. V. Shokhirev, *J. Chem. Phys.*, **96,** 1951 (1991).
29. E. Haas, E. Katchalski-Katzir, and I. Z. Steinberg, *Biopolymers*, **17,** 11 (1978).
30. I. Z. Steinberg, *J. Theor. Biol.*, **166,** 173 (1994).
31. F. C. Goodrich, *J. Chem. Phys.*, **22,** 588 (1954).
32. N. Agmon, *J. Chem. Phys.*, **81,** 2811 (1984).
33. E. Pines, D. Huppert, and N. Agmon, *J. Chem. Phys.*, **88,** 5620 (1988).
34. D. Huppert, E. Pines, and N. Agmon, *J. Opt. Soc. Amer. B*, **7,** 1545 (1990).
35. N. Agmon, D. Huppert, A. Masad, and E. Pines, *J. Phys. Chem.*, **95,** 10407 (1991); erratum, **96,** 2020 (1992).
36. T. Förster and S. Völker, *Chem. Phys. Lett.*, **34,** 1 (1975).
37. M. Hauser, H.-P. Haar, and U. K. A. Klein, *Ber. Bunsenges. Phys. Chem.*, **81,** 27 (1977).
38. H.-P. Haar, U. K. A. Klein, and M. Hauser, *Chem. Phys. Lett.*, **58,** 525 (1978).
39. Z. Schulten and K. Schulten, *J. Chem. Phys.*, **66,** 4616 (1977).
40. A. A. Zharikov and N. V. Shokhirev, *Z. Phys. Chem. NF*, **177,** 37 (1992).
41. E. B. Krissinel', N. V. Shokhirev, and A. M. Raitsimring, *High Energy Chem.*, **23,** 316 (1989).
42. A. I. Burshtein, *Soviet Phys. Uspekhi*, **27,** 579 (1984).
43. A. Szabo, *J. Phys. Chem.*, **93,** 6929 (1989).
44. L. Song, R. C. Dorfman, S. F. Swallen, and M. D. Fayer, *J. Phys. Chem.*, **95,** 3454 (1991).
45. R. C. Dorfman and M. D. Fayer, *J. Chem. Phys.*, **96,** 7410 (1992).
46. A. I. Burshtein, E. B. Krissinel', and M. S. Mikhelashvili, *J. Phys. Chem.*, **98,** 7319 (1994).
47. D. Huppert, S. Y. Goldberg, A. Masad, and N. Agmon, *Phys. Rev. Lett.*, **68,** 3932 (1992).
48. N. Agmon, *Phys. Rev. E*, **47,** 2415 (1993).
49. A. Szabo, *J. Chem. Phys.*, **95,** 2481 (1991).
50. N. Agmon and A. L. Edelstein, *J. Chem. Phys.*, **100,** 4181 (1994).
51. R. Kosloff and H. Tal-Ezer, *Chem. Phys. Lett.*, **127,** 223 (1986).
52. C. Canuto, M. Y. Hussaini, A. Quarteroni, and T. A. Zang, In *Spectral Methods in Fluid Dynamics, Springer Series in Computational Physics*, J.-L. Armand et al., Eds., Springer-Verlag, New York, 1988.
53. F. R. Gantmakher, *Matrix Theory*, Nauka, Moscow, 1988.
54. G. Wilemski and M. Fixman, *J. Chem. Phys.*, **58,** 4009 (1973).
55. M. Abramowitz and I. A. Stegun, Eds., *Handbook of Mathematical Functions*, Dover, New York, 1970.
56. U. M. Gösele, *Prog. React. Kinet.*, **13,** 63 (1984).
57. M. Gitterman and G. H. Weiss, *Chem. Phys.*, **180,** 319 (1994).
58. G. H. Weiss, *J. Chem. Phys.*, **80,** 2880 (1984).
59. M. Gitterman and G. H. Weiss, *Chem. Phys. Lett.*, **193,** 469 (1992).
60. N. Agmon, *J. Chem. Phys.*, **90,** 3765 (1989).